Available online at www.sciencedirect.com
ScienceDirect
Polymer 48 (2007) 616–623
polymer
www.elsevier.com/locate/polymer

Mechanism for compression set of TDI polyurethane foams

Mark F. Sonnenschein [a,*], Robbyn Prange [b], Alan K. Schrock [b]

[a] Corporate Research and Development, The Dow Chemical Company, 1702 Building, Midland, MI 48674, United States
[b] Performance Chemicals and Plastics R&D, The Dow Chemical Company, Freeport, TX 77541, United States

Received 23 August 2006; received in revised form 8 November 2006; accepted 9 November 2006
Available online 6 December 2006

Abstract

A model is presented in which compression set of TDI foams is a result of thermal and stress-induced relative flow of the hard and soft phase following hydrogen bond disruption. The majority of the soft segment consists of a mobile phase that exhibits liquid-like dynamics. However, a significant fraction of the soft segment is immobilized due to hydrogen bond interactions with the phase-separated polyurea hard segment. As temperature is increased, the hydrogen bonding between the soft and hard segment progressively weakens until there is little or no interaction and the phases are free under stress to flow past each other. FTIR data do not indicate that changes in the hard–soft phase interactions are accompanied by changes in intra-hard segment hydrogen bonding. Upon cooling, the hard–soft segment hydrogen bond interactions can re-establish themselves in a new compressed geometry if the phase separated, co-continuous hard segment does not provide sufficient restorative force to regain the initial dimensions. This model is based on data obtained by DSC, SEM, temperature-dependent FTIR, solid state NMR, SAXS and compression set measurements.

Keywords: Polymer physics; Flexible foams; Compression set

1. Introduction

Polyurethane foams are ubiquitous in our day-to-day lives. Their structure and properties have been extensively explored by many workers [1,2] and the field has developed a significant amount of conventional wisdom [3]. One fundamental property of polyurethane foam is the tendency to undergo non-recoverable deformation under a defined compressive load, exacerbated by temperature and humidity. This phenomenon is commonly referred to as compression set. Compression set is so crucial that many individual manufacturers and end users have established specific tests and criteria to qualify the acceptability of specific foam samples. Fundamentally, compression set has been shown to result from stress-induced deformation of the polyurethane co-continuous hard phase [4], decomposition of the urethane bond [5], and hard segment slippage through the co-continuous soft phase [5]. In humid environments, compression set has been ascribed to plastization [6] and disruption of the hard segment [7] or soft segment hydrogen bonding [8,9]. Certainly, all of these phenomena can occur and under some circumstances will occur, however, it has previously been shown that compression set is a strongly temperature-dependent process with clear and dramatic threshold behavior [10]. Thus, two foams that may be in most respects quite similar can in a specific test yield very different compression set values simply resulting from the sensitivity of the phenomenon to the test conditions. The purpose of this paper is to provide additional insight into the molecular level phase interactions that occur below, at and above the typical compression set test temperatures. Employing analytical methods including microscopy, differential scanning calorimetry (DSC), Fourier transform infrared spectroscopy (FTIR), solid state nuclear magnetic resonance (NMR) spectroscopy, and X-ray crystallography, we propose a mechanism for compression set in these foams in which the dynamics are controlled by an immobile soft segment phase which is strongly interacting with the hard segment phase through hydrogen bonds [11,12]. These bonds weaken as temperature is increased [4,13,14] and at a sample-dependent temperature, the hard segment phase can move relative to the soft segment

* Corresponding author. Tel.: +1 989 636 7415; fax: +1 989 636 4019.
E-mail address: mfsonnenschein@dow.com (M.F. Sonnenschein).

0032-3861/$ - see front matter © 2006 Elsevier Ltd. All rights reserved.
doi:10.1016/j.polymer.2006.11.021

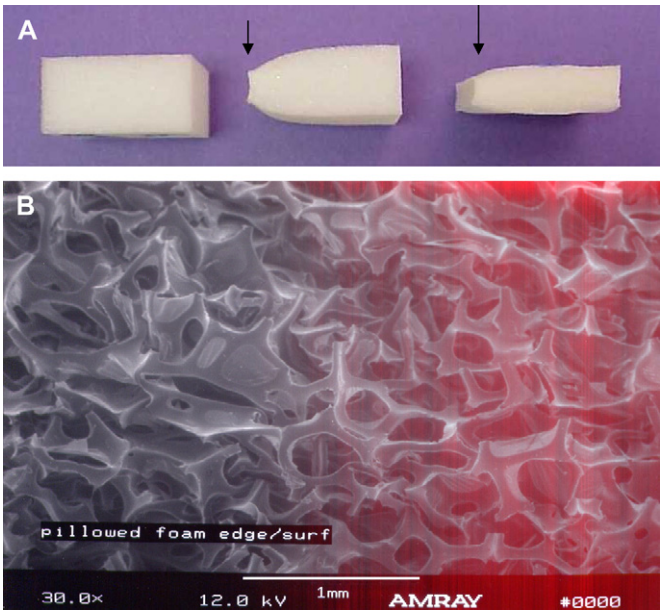

Fig. 1. (A) Foams exhibiting different amounts of compression set following testing according to ASTM D3574 Test D and SEM of deformed areas such as indicated by the arrows. (B) SEM of the foam in a section exhibiting high compression set.

phase. When the temperature is reduced, the hard and soft segment phases will resume their hydrogen bonding interactions in the new deformed geometry. These forces may be weak relative to the overall strength of the hard segment's restoring force [14–19] and foams with better hard segment segregation [20,21] are observed to recover their original dimensions. However, at low enough temperatures all foams evidence very low compression set and at high enough temperatures all foams have poor compression set values.

The concept of a foam's ''restoring force'' is not usually invoked because the stress or modulus is usually substituted. However, the anisotropy of forces in foam compression as evidenced in Fig. 1 indicate that an area normalized parameter such as modulus may not be satisfactory to describe the state of a material with finite dimensions. Fig. 1 unambiguously demonstrates that the stresses at the edges of samples may be significantly different than those at the center, especially at high strains, and may also be a function of the gross geometry of the sample. In this case, the restoring force is expressed simply as Eq. (1) where E is the strain-dependent Young's modulus, ε is the strain and A is the cross-sectional area of a given volume element.

$$F = E(\varepsilon)\varepsilon A \tag{1}$$

2. Experimental

2.1. Materials

All polyols and toluene diisocyanate (an 80/20 mixture of the 2,4 and 2,6 isomers) (TDI) were obtained from Dow Chemical, Freeport, Texas. The structural information is in Table 1. DABCO 33LV catalyst was obtained from Air Products (Allentown, PA). Diethanolamine (DEOA) was obtained from Aldrich (Milwaukee, WI). NIAX A-1 catalyst, Niax A-300 catalyst and NIAX Y-10184 silicone surfactant were obtained from OSi Specialties Witco (Now GE Silicones, Wilton, CT). Distilled or deionized water was used as a reactant to produce CO_2 in the foaming process.

Table 1
Relevant structural information on polyols and isocyanates used in these experiments

Polyol or TDI	Equivalent weight	%EO	Functionality
VORANOL VORACTIV™[a]	1700	17.5	4
SPECFLEX™ NC630 polyol	1810	15.5	3
XSS 84804.01 polyol	1810	17	3
VORACTIV 6340 polyol[b]	1750	17.2	3.6
VORANATE™ T-80 TDI	87		2

[a] This polyol is initiated with 3′-diamino-*N*-methyldipropylamine giving it intrinsic catalytic properties within the foaming process. This polyol is currently available from Dow under the tradename VORACTIV polyol.
[b] A 60/40 (w/w) blend of VORACTIV and XSS 84804.01 polyols.

2.2. Foam formulation and preparation

Polyol master batches (typically 34 kg, formulations listed in Table 2) were prepared in a 20 gallon phenolic-coated steel kettle. The master batch containing polyols, surfactant, crosslinker, catalyst, and water was stirred for 30 min at approximately 600 rpm. After mixing was completed, the master batch was transferred to the polyol tank of a Canon A-40 foaming machine. The polyol master batch was allowed to circulate for an additional 30 min to allow it to come to thermal equilibrium (25 °C). The polyol master batch and the toluene diisocyanate (TDI) streams were mixed at a high speed impingement mixing head prior to being dispensed into a heated in a mold (38.1 cm × 38.1 cm × 11.4 cm). The molar ratio of isocyanate to active hydrogen (from polyol and water) was 1.05 in all cases except one where it was 0.90. Nominal throughput of the machine was 155 g/s at the component ratios

Table 2
Foam formulations for experiments in this work

Component	Description	CNTR	VOR	VOR/A-300
NC630	See Table 1	62.5	0.00	0.00
VORACTIV 6340	See Table 1	0.00	62.5	62.5
SPECFLEX NC700	Copolymer polyol (40% solids)	37.5	37.5	37.5
Niax Y-10184	Silicone surfactant	1.2	1.0	1.0
Diethanolamine	Crosslinker	1.6	1.6	1.6
Dabco 33LV	Catalyst for urethane formation (gelation)	0.35	0.3	0.00
Niax A-300	Time delayed gelation catalyst	0.00	0.00	0.30
Niax A-1	Catalyst for urea formation (blowing)	0.08	0.00	0.00
Water	Blowing agent	4.2	4.2	4.05
Total		107.43	107.1	106.95

Niax A-300 contains 50% water, thus the VOR/A-300 formulations contain 4.2 parts water.

necessary to maintain an isocyanate to hydroxyl ratio of 1.05. All foams were subsequently cured at 155 °C for 6.5 min. After the foam was removed from the mold (aided by a silicone mold release) the foam was crushed to 5, 3.75 and 2.5 cm. Foam properties were measured on 38 cm × 38 cm × 11.5 cm pads cut from the center of the resulting pad following 7 days of room temperature aging. Each sample is the result of 3–6 foam specimens. Qualitatively, there was no visual difference among the foams and all foams had similar vent times (25–27 s), the time at which the rising foam escapes through the mold vents after completely filling the mold. One foam is designated as a control foam because it does not possess a mixed polyol system. The use of A-300, a delayed gelation catalyst, is used to probe the effects of enhanced phase separation on the resulting set properties.

2.3. Test methods

Dry aged compression set at 75% compression was obtained in accordance with ASTM D3574 Test D [22]. This test was also altered and run at different temperatures. Each test was done in triplicate. In addition, air flow and density were measured on each foam specimen. Compression set samples were measured by the following procedure. Three 5 × 5 × 2.5 cm samples of foam, cut from the same 1x test pad were compressed 75% at various temperatures for 22 h. Compression was uniformly applied in a jig designed to uniformly and precisely compress the foam across its entirety. After the 22 h compression, the foams were allowed to recover for 30 min at ambient conditions. The recovered height was then measured and the deflected compression value (C_d) was calculated as

$$C_d = \frac{H_o - H_f}{H_o - H_s} \times 100 \quad (2)$$

where H_o is the original height of the sample, H_f is the final height of the sample and H_s is the compressed height (75% of H_o).

Small angle X-ray scattering (SAXS) analyses for *d*-spacing were performed using the following procedure. Foam samples were cut to a width of 5 mm and placed in the Kratky camera under vacuum. The Kratky camera was aligned with a vertical X-ray tube stand where Cu K_{avg} radiation $\lambda = 1.54184$ Å was transmitted through the sample. SAXS from the sample traveled down the waveguide 72 cm where data were collected with a position sensitive detector. SAXS data were collected for 30 min through a q ranging from 0.01 $Å^{-1}$ to 0.138 $Å^{-1}$ which corresponds in *d*-space from 628 Å to 45.6 Å. SAXS data were analyzed using JADE XRD pattern processing software. Profile fit analyses were performed on the intensity spectra and Lorentz (Iq^2) corrected data. Both methods yielded comparable trends with *d*-spacings from the Lorentz corrected data giving somewhat smaller absolute but generally more precisely determined values. Although the Lorentz correction is primarily reserved for lamellar crystalline structures, some have reported the polyurethane hard segment phase in slab stock foams to be ''lamellar like'' [15].

Foam extractions were performed on samples weighing approximately 0.5 g. Samples were placed in extraction thimbles and continuously Soxhlet extracted with either THF or DMF for a minimum of 8 h. Swollen samples were subsequently allowed to evaporate solvent for at least 24 h or until the weight change was less than 0.001 g. Weight change was then calculated by inserting initial and final foam sample weights into the equation.

$$1 - \frac{w_f}{w_i} \quad (3)$$

Samples extracted with DMF were occasionally more difficult to analyze due to the very strong swelling and subsequent softening that occurred. All foams lost 8 ± 0.5% of their initial weight indicating that compression set was not a result of differences in component conversion to polymer.

DSC was performed using a TS DSC 2920. Foam specimens (10–15 mg) were enveloped in aluminum pans under dry N_2. The scanning rate was 10 °C/min from −120 to 200 °C. To insure that no water was present in the foam, three temperature cycles were executed.

Temperature-dependent infrared spectroscopy of foams was performed using a Perkin–Elmer Paragon 1000 FTIR spectrometer. Spectra were collected in transmission using very thin slices (~1 mm thickness) of the dry foam held between KBr (Aldrich) circular plates. The foam assembly was fixtured in a homemade resistively heated insulated brass cell held in the film sample holder under a continuous dry N_2 purge. Foams were allowed to achieve the specified temperature and equilibrated for 15 min before taking the spectrum. Spectra represent the average of 16 scans.

All solid state NMR spectra were collected on a Varian Chemagnetics CMX-360 spectrometer using a Doty 5 mm double resonance MAS probe. The ^1H and ^{13}C resonance frequencies were 360.24 and 90.598 MHz, respectively. The magic angle spinning rates were 8.5 kHz unless otherwise specified. High-power proton de-coupling (56 KHz) was employed during the detection period for ^{13}C CP/MAS experiments.

3. Results and discussion

In the past, there had been speculation that macroscopic properties of foams such as air flow were directly related to foam compression set [10,23]. However, it has since been recognized that molecular structure is the relevant size scale for understanding compression set, and variables such as closed cell content are just symptomatic of the underlying polymer structure resulting from the polymerization reactions that occur during foaming [5–7,24]. Thus, we need first to identify foams with differential compression set properties, and subsequently detect the polymer structural properties intimately associated with the phenomena. In fact there is no problem identifying foams with substantially different compression set properties. The foams exhibited in Fig. 1

illustrate different extents of compression set with one showing little or no compression set, the middle one with deformation of an edge, and a severely deformed foam on the right. SEM (Fig. 1B) shows that high compression set foams have a distorted cell structure, but does not suggest that there is any adhesive interaction between the struts as might occur if there was substantial molecular weight loss.

Numerous workers have empirically determined that formulation modification can result in large differences in compression set values [2,5–8,10]. Since the compression set test is performed under specific conditions, it might be a mistake to assume that compression set is an intrinsic property of the polymer rather than a value which may be very sensitive to small systematic variations *in the test*. Thus we find data for compression set for foams in Fig. 2 consistent with that found previously [10], albeit for different compositions. Our work also confirms previous observations that variables such as isocyanate index ([NCO]/[OH]) [7], annealing [10,25,26], and differences in catalyst [10] can substantially affect compression set at 70 °C. However, it is just as revealing that compression set measurements made at other temperatures evidence much more similarity among these foams. For instance, if instead of 75 °C or 80 °C, the measurements were made at 90 °C or 65 °C we would be led to judge these foams as insignificantly different. Furthermore, in many instances, physically manipulating compressed foams such as in Fig. 1 will restore the foam to its initial shape. Thus, we are interested in identifying polymer dynamics that have a similar thermal profile, and perhaps even activation energy as that suggested in Fig. 2, and design structures that may systematically alter the measured performance quantified in Fig. 2.

DSC provides an alternative view of the process [4,26–28]. Fig. 3 is the DSC data for the three foams specified in Table 2 and Fig. 2. It is clear that these foams are quite similar in many respects based on the similar soft segment glass transition temperature at ca. −55 °C and the similar change in heat capacity at this transition. The DSC scans also show that for three foams with different compression set properties, the polymer is expressing a change in heat capacity in the relevant temperature range defined in Fig. 2. However, all three foams are describing behavior with some change beginning at about 30 °C and finishing at about 100 °C. While this measurement

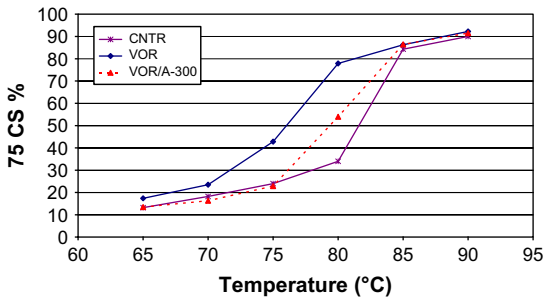

Fig. 2. Temperature-dependent compression set of the three foams described in Table 2.

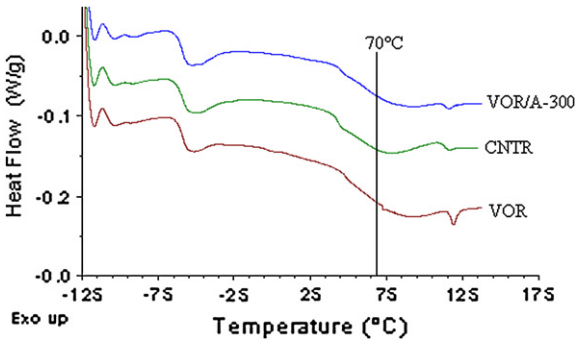

Fig. 3. DSC scans of the foams described in Table 2.

does not exhibit the same temperature dependence as the compression set values in Fig. 2, it does suggest that there is some enthalpic alteration of the polymer structure occurring in these foams with a maximum rate at about 70 °C. The obvious possibility that we are observing water evaporation is negated by our observation that the thermal profile and its intensity is unaffected by drying the foams at 100 °C in a vacuum oven for 24 h or by running consecutive DSC scans.

Infrared spectroscopy has been used in the past to probe polyurethane structure because many of the vibrational resonances are well known and are sensitive to structural variations [29–31]. When polyurethane foams of the current experiments are interrogated over the temperature range 25–85 °C only one band is observed to exhibit significant temperature sensitivity, that being the N–H band, particularly that part of the resonance extending from 3450 to 3650 cm^{-1} (the bidentate urea peak at 1645 cm^{-1} shows a slight increase that is not reversible). Like the DSC data, the FTIR data show qualitatively similar behavior for two foams that have significantly different compression sets measured at 70 °C. However, this result suggests that the N–H bond of polyurea isolated in the soft segment and polyurea in the hard segment is involved in a thermal transition. The high resonance energy of the affected population indicates that it is minimally stabilized in the ground state by hydrogen bonding. This region of the resonance has sometimes been identified with an isolated N–H stretch [32,33]; however, recent work in cold gas expansions puts the isolated N–H stretch at about 3550 cm^{-1} [34–37]. In the present case, the affected resonance extends out to 3650 cm^{-1} and overlaps the OH resonance from the dry polyol (not shown). However, this N–H resonance has been observed in other studies [26,30,38] in which no OH is structurally available [25,32,39], and has also evidenced the same temperature dependence as observed in the present experiments [26]. Furthermore, while temperature-dependent FTIR spectroscopy of the polyols over the same temperature range does show a reduction and blue shifting of intensity, the result is in no way as dramatic as that seen in Fig. 4.

In the present case, it seems likely that the temperature-dependent IR resonance in question is a result of hydrogen bond interactions of hard segment N–H with the soft segment ether linkages and any possible remaining hydroxyl from unreacted soft segment at the highest frequencies. Furthermore,

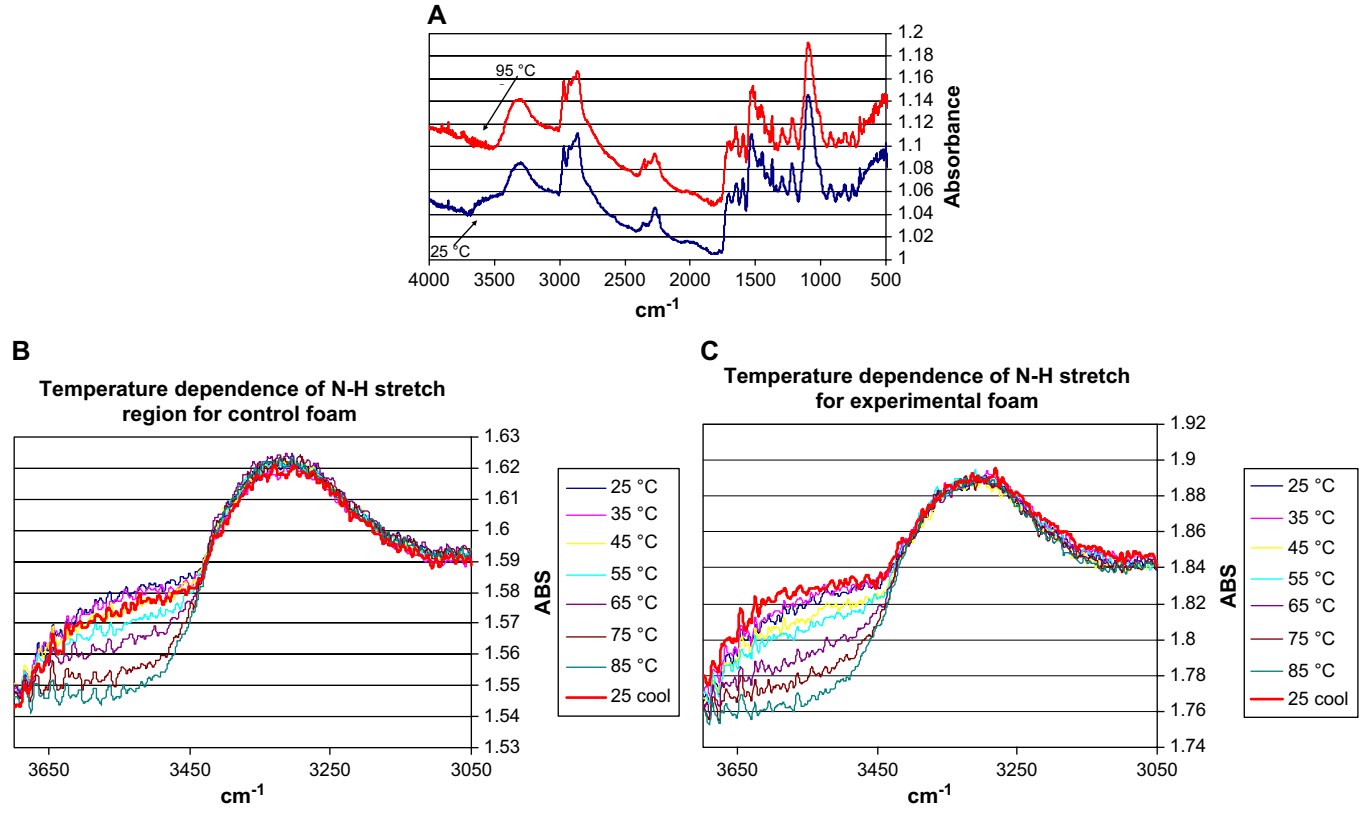

Fig. 4. FTIR of (A) CNTR foam at 25 °C and 95 °C; (B) temperature step study of the CNTR foam N–H resonance from 25 °C to 85 °C; (C) temperature step study of the VOR foam N–H resonance from 25 °C to 85 °C.

the FTIR data, like the DSC data, reveal a continuous process occurring in the foams that does not have the same functional dependence as the compression set of the foams shown in Fig. 2. Also, like the DSC, the FTIR data reveals a process that is finished or nearly so by the temperature at which all foams show uniformly high compression set values. Lastly, there does not appear to be a substantial alteration in the intra-hard segment hydrogen bonding in this temperature range as reported by the N–H resonance between 3100 and 3450 cm^{-1} [28].

An additional way to probe the chain dynamics of PU systems is to employ solid state NMR techniques [9,25,40–42]. In particular, the magnitude of the proton dipolar coupling is very sensitive to relatively slow molecular motions in solids. This method combined with the Hahn spin-echo technique was used to quantify the molecular mobility of the soft segments. A stacked plot of the ^1H MAS NMR spectra of the VOR foam acquired with varying ^1H dipolar-dephasing time is shown in Fig. 5 as well as an example of the curve fitting used to derive the dephasing components. The dipolar-dephasing time constants were determined from the least-square fit of the NMR peak intensity versus dipolar-dephasing time. The dipolar-dephasing curve was fit with two exponential components. This indicates that the soft segments consist of two components with significantly different molecular mobility. The terms "fast" and "slow" were used to describe multiple dipolar-dephasing components as shown in Table 3. It is hypothesized that the two phases of the soft segment consist of

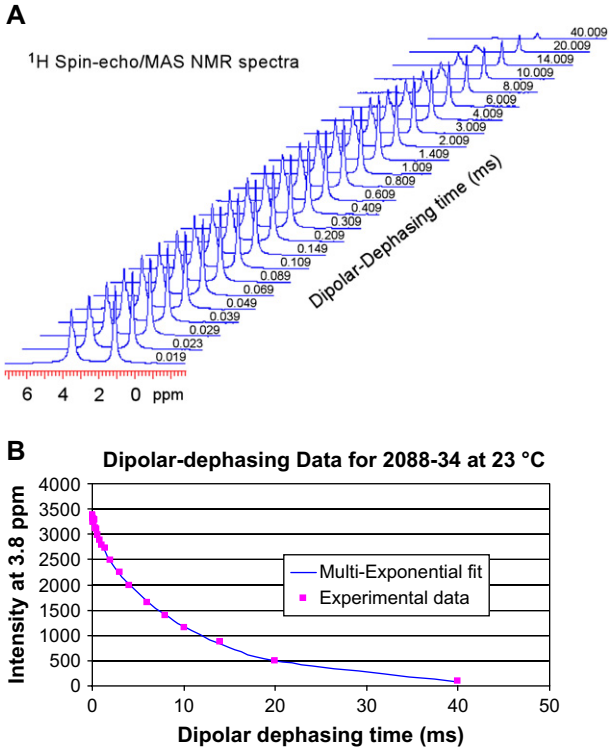

Fig. 5. (A) Representative stack plot of ^1H MAS NMR spectra of the VOR foam acquired at 38 °C with values of the ^1H dipolar-dephasing time indicated using the Hahn spin-echo technique. (B) Representative bi-exponential fit to data obtained from stack plot data.

Table 3
Proton dipolar-dephasing time constants determined for (A) CNTR, (B) VOR and (C) VOR/A-300 foams

Temp. (°C)	3.8 ppm				3.6 ppm				1.4 ppm			
	P_f (%)	T_{df} (ms)	P_s (%)	T_{ds} (ms)	P_f (%)	T_{df} (ms)	P_s (%)	T_{ds} (ms)	P_f (%)	T_{df} (ms)	P_s (%)	T_{ds} (ms)
A: CNTR foam												
38	15.8	1.76	84.2	11.5	28.7	1.76	71.3	11.8	15.7	2.55	84.3	15.3
68	14.0	0.50	86.0	17.1	19.4	0.50	80.6	17.7	16.0	0.50	84.0	25.4
87	5.8	0.20	94.2	20.0	3.8	0.22	96.2	21.2	5.0	0.18	95.0	31.8
B: VOR foam												
38	26.4	1.78	73.6	12.0	36.7	1.75	63.3	12.8	25.9	2.55	74.1	15.5
68	3.4	0.50	96.6	15.9	6.9	0.50	93.1	15.9	4.4	0.50	95.6	22.7
87	–	–	100.0	18.5	–	–	100.0	18.5	0.8	0.20	99.2	27.8
C: VOR/A-300 foam												
38	31	1.76	69.0	11.8	39.7	1.76	60.3	12.0	26.2	2.55	73.8	14.7
68	8.3	0.50	91.7	15.2	8.3	0.50	91.7	15.2	5.4	0.50	94.6	21.3
87	6.3	0.2	93.7	18.1	12.6	0.22	87.4	18.2	4.7	0.18	95.3	27.2

Chemical shift designations refer to peaks shown in Fig. 5.

(1) a true mobile phase (slow segment) and (2) a restricted soft segment phase that is at the interface of the hard and soft segments. It is considered that these two components are spatially separated since ^{1}H spin diffusion cannot effectively average the different dynamical behaviors of protons in different spatial domains on the time scale of T_d. The minimal domain size is estimated to be in the order of 1 nm. The data show that the percentage of the ''slow'' (truly mobile phase) segment (P_s) and the slow segment dipolar-dephasing time constant (T_{ds}) increased when the temperature was raised (Table 3). This is expected since increasing temperature promotes polymer chain motion. However, the dipolar-dephasing time constant of the fast dephasing component (T_{df}) actually decreased with rising temperature. This can be explained by the fact that T_{df} is an average value of the dipolar-dephasing time constants of protons in a small domain via the proton spin diffusion process. At higher temperature, the spin diffusion process is less efficient averaging out the T_d differences so it is easier to detect the less mobile slow segment dipolar-dephasing time constant (T_{ds}) when the temperature is raised (Table 3). As mentioned earlier, it is likely that the fast dephasing component detected above 68 °C is the soft segment component that is at or close to the interface of the hard and soft segments, thus its mobility is restricted by the adjacent hard segment. The major difference between the foam samples in Table 3 is the percentage of the fast dephasing (P_f) component at various temperatures. The VOR and VOR/A-300 have higher P_f than the CNTR at 38 °C (immobilized soft segment). However, at 87 °C the CNTR and VOR/A-300 have higher P_f than the VOR foam. In fact, solid state NMR did not detect any restricted phase soft segment (P_f) in the VOR foam at 87 °C. In other words, the soft segment in the VOR foam is more mobile than the CNTR and VOR/A-300 foams at 87 °C and also exhibits poorer compression set proprieties at 70 °C. The data suggest that the soft segment of all these foams obtains additional motional degrees of freedom at temperatures above 60 °C, and that the affected soft segment is associated with the polyurea hard segment. Due to this hard segment–soft segment interaction, the temperature at which this motion proceeds is a function of hard segment features such as volume fraction and degree of phase separation from soft segment [4,6,7,20,21,43,44].

Consistent with this observation is the relatively strong correlation between compression set and small angle X-ray (SAXS) determined *d*-spacing (Fig. 6); a measure of the distance between hard segment domains and degree of phase separation for foams with equal volumes of hard segment. In these experiments, the hard segment volume (the volume of water and isocyanate to the overall volume of the solid mass) was maintained constant so that an increase in *d*-spacing correlates directly to enhanced phase separation and increased hard segment size. The *d*-space data indicate that foams with more complete phase separation, and phase separation into larger domains, are optimized to minimize compression set. This picture is consistent with polyurethane models in which hard segments form a co-continuous phase with the soft segment which is certainly the case in the present foams having approximately 33% hard segment volume. This co-continuous hard segment phase not only increases the polymer modulus but increases the foam's restoring force to recover its initial shape. The use of a third phase crystalline component in thermoplastic polyurethanes has been shown to result in a similar effect [24,44].

The accumulated data suggest a unique model for molecular level processes occurring to PU foam under deformation. The foam at room temperature is conventionally described as low T_g soft segment and high T_g phase-separated hard segment. However, the NMR data presented indicate that there is a third phase of immobilized polyol possessing dynamics at room temperature more similar to the hard segment. The FTIR data suggest that this interaction is mediated through hydrogen bond interactions primarily between the N–H provided by the urea hard segment, and the non-bonded electrons of the soft segment ether groups [45]. At elevated temperature and sufficient deformation, the hard–soft segment interactions are weakened to the point that large scale flow is initiated between the phases (Fig. 2). These hard–soft interactions are enthalpic in nature and their destruction requires a net

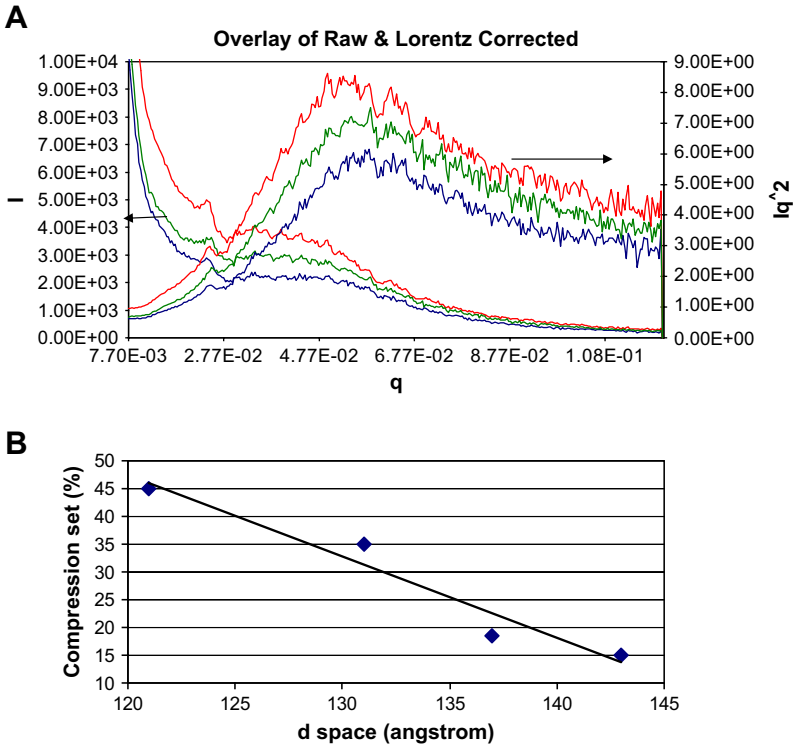

Fig. 6. (A) Raw spectral SAXS data (I) and Lorentz corrected (Iq^2) spectra for polyurethane foams. The Lorentz corrected data have been deconvoluted from the unscattered beam intensity. The peak at $q = 0.24$ is an artifact of the camera set-up and not meaningful. (B) 75% Compression set at 70 °C as a function of foam d-spacing from uncorrected spectra (all foams have the same isocyanate index and the same hard segment volume).

input of energy as seen by DSC. If the co-continuous hard phase does not provide adequate restoring force, the foam will maintain its new conformation and as the temperature of the foam decreases new hard–soft segment interactions may form as shown by the FTIR data. However, if the hard segment does provide adequate restoring force by such means as by improved phase separation (as evidenced by larger d-spacing) then the new hard–soft segment interactions may be overcome and the foam can resume most or all of its previous geometry. This compression set model is consistent with dynamic aspects previously suggested by Koberstein et al. [4], Wilkes et al. [6,8,21] and Palmer et al. [31], but provides a more specific physical/structural model, and also provides evidence of a sensitive threshold behavior for the processes occurring in a compression set experiment. Initial deformations occur at the edge because of the two-dimensional restoring forces experienced at the edges as opposed to the three-dimensional isotropic forces at the center. Furthermore, due to the decreasing restoring force away from the center of the sample, it may be that simply changing the geometry (to thicker sample sizes for instance) may influence the onset of compression set behavior. In the present case; all the foams perform in a qualitatively similar manner and accurate measurement of these systems can be extremely sensitive to systematic errors in temperature and in applied load. The data from the experiments are consistent with this model, but the NMR, DSC and FTIR suggest that there is a continuous process of weakening hard–soft segment interaction that occurs before the foams ever evidence their fundamental differences with respect to the compression set test. The sudden onset for change in measured compression set suggests however, that there is a threshold level of hard–soft segment interaction that must be disrupted before the large-scale motions can commence. Alternatively, it may be that the gross phase structure that results in compression set changes is most influenced by the most strongly interacting hard and soft segments interactions that are disrupted at the highest temperatures.

4. Conclusions

The physical phenomena accompanying PU foam compression reflects the threshold temperature at which interactions at the hard–soft segment interface are weakened sufficiently to allow large-scale flow under deformation. These interactions involve hydrogen bonds between N–H of the hard segment urea phase with the polyol ether or hydroxyl oxygens. Changes in the hydrogen bond strength can be followed by numerous analytical methods, but compression set exhibits highly nonlinear thermal dependence reflecting a critical decrease in phase interaction that must be achieved to result in permanent deformation. Better hard segment phase separation allows the foam to re-establish its initial geometry due to the increased restoring force that thicker hard segment can provide.

Acknowledgements

The authors would like to thank Dr. J. Xiong for help with the NMR experiments, Mr. Danny King for help with the SAXS experiments, Drs. David Babb and Douglas Brune for helpful discussions, Drs. Marianne McKelvy and Robert Zeigler are thanked for a thorough review of this manuscript and the Dow Chemical Company for its support of this research. VORANOL, VORANOL VORACTIV, VORANATE, and SPECFLEX are trademarks of The Dow Chemical Company.

References

[1] Smith CH, Degisi SL. J Appl Polym Sci 1966;10:795–805.
[2] Van der Schuur M, van der Heide E, Feijen J, Gaymans RJ. Polymer 2004;45:2721–7.
[3] Hock K, Priester R, Herrington R, Wiltz G, Jeng L. In: Herrington R, Hock K, editors. Dow polyurethanes flexible foams. 2nd ed. Midland, MI: Dow Chemical Pubs; 1997 [chapter 7].
[4] Koberstein JT, Galambos AF, Leung LM. Macromolecules 1992;25: 6195–204.
[5] Moreland JC, Wilkes GL, Turner RB. J Appl Polym Sci 1994;52: 549–68.
[6] Dounis DV, Wilkes GL. Polymer 1997;38:2819–28.
[7] Dounis DV, Wilkes GL. J Appl Polym Sci 1997;66:2395–408.
[8] Kaushiva BD, Dounis DV, Wilkes GL. J Appl Polym Sci 2000;78: 766–86.
[9] Horstmann M, Urbani M, Veeman W. Macromol Symp 2004;205: 129–42.
[10] Skorpenske RG, Solis R, Kuklies RA, Schrock AK, Turner RB. Proc SPI Annu Tech Mark Conf 1992;34:650–9.
[11] Blackwell J, Gardner KH. Polymer 1979;20:13–7.
[12] Beck RA, Truss RW. J Appl Polym Sci 1999;71:959–66.
[13] Wang H, Thompson DG, Schoonover JR, Aubuchon SR, Palmer RA. Macromolecules 2001;34:7084–90.
[14] Seefried CG, Koleske JV, Critchfield FE. J Appl Polym Sci 1975;19: 2503–13.
[15] Li W, Ryan AJ, Meir IK. Macromolecules 2002;35:6306–12.
[16] Sonnenschein MF. J Polym Sci Polym Phys Ed 2003;41:1168–74.
[17] Aneja A, Wilkes GL. J Appl Polym Sci 2002;85:2956–67.
[18] Martin C, Eeckhaut G, Mahendrasingham A, Blundell DJ, Fuller W, Oldman RJ, et al. J Synch Rad 2000;7:245–50.
[19] Gibson LJ, Ashby MF. Cellular solids. 2nd ed. Cambridge, UK: Cambridge University Press; 1997. p. 237–8.
[20] Armistead JP, Wilkes GL, Turner RB. J Appl Polym Sci 1988;35: 601–29.
[21] Ophir Z, Wilkes GL. J Polym Sci Polym Phys Ed 1980;18:1469–80.
[22] Standard test methods for flexible cellular materials. Philadelphia: American Society for Testing and Materials D3574-05; 2005.
[23] Herrington R, Hock K, editors. Dow polyurethanes flexible foams. 2nd ed. Midland, MI: Dow Chemical Pubs; 1997. C2.
[24] Sonnenschein MF, Lysenko Z, Brune DA, Wendt BL, Schrock AK. Polymer 2005;46:10158–66.
[25] Christenson CP, Harthcock MA, Meadows MD, Spell HL, Howard WL, Creswick MW, et al. J Polym Sci Part B Polym Phys 1986;24:1401–39.
[26] Ning L, De-Ning W, Sheng-Kang Y. Macromolecules 1997;30: 4405–9.
[27] Martin DJ, Meijs GF, Rewick GM, McCarthy SJ, Gunatillake PA. J Appl Polym Sci 1996;62:1377–86.
[28] Harrell LL. Macromolecules 1969;2:607–12.
[29] Elwell MJ, Ryan AJ, Grunbauer HJM, Van Liehout HC. Polymer 1996; 37:1353–61.
[30] Kim HD, Huh JH, Kim EY, Park CC. J Appl Polym Sci 1998;69: 1349–55.
[31] Wang H, Aubuchon SR, Thompson DG, Osborn JC, Marsh AL, Nichols WR, et al. Macromolecules 2002;35:8794–801.
[32] Tobin MC, Carrano MJ. J Chem Phys 1956;25:1044–52.
[33] Trifan DS, Terenzi JF. J Polym Sci 1958;28:443–5.
[34] Wu CC, Jiang JC, Hahndorf I, Chaudhri C, Lee YT, Chang HC. J Phys Chem A 2000;104:9556–65.
[35] Florio GM, Zwier TS. J Phys Chem A 2003;107:974–83.
[36] Chin W, Mons M, Dognon J-P, Mirasol R, Chass G, Dimicoli I, et al. J Phys Chem A 2005;109:5281–8.
[37] Oh H-B, Lin C, Hwang HY, Zhai H, Breuker K, Zabrouskov V, et al. J Am Chem Soc 2005;127:4076–83.
[38] Seymour RW, Estes GM, Cooper SL. Macromolecules 1970;3:579–83.
[39] Luo N, Stewart MJ, Hirt DE, Husson SM, Schwark DW. J Appl Polym Sci 2004;92:1688–94.
[40] Szayna V, Voelkel R. Solid State Nucl Magn Reson 1999;15:99–102.
[41] Ghose S, Isayev AI, von Meerwall E. Polymer 2004;45:3709–20.
[42] Cardenas G, Cabrera G, Taoada E, Miranda SP. J Appl Polym Sci 2004; 93:1876–85.
[43] Stribeck N. In: Faikirov S, editor. Handbook of condensation thermoplastic elastomers. Weinheim: Wiley-VCH; 2005 [chapter 7].
[44] Korley LT, Pate BD, Thomas EL, Hammond PT. Polymer 2006;47: 3073–82.
[45] Yokoyama T. In: Frish KC, Reeger SL, editors. Advances in urethane science and technology. Westport, CT: Technomica Pub; 1978. p. 1–29.